Journal of Rock Mechanics and Geotechnical Engineering 15 (2023) 1076–1089

Contents lists available at ScienceDirect

Journal of Rock Mechanics and Geotechnical Engineering

journal homepage: www.jrmge.cn

Full Length Article

Numerical modelling of resonance mechanisms in jointed rocks using transfer functions

Harry Holmes [a,*], Chrysothemis Paraskevopoulou [a], Mark Hildyard [a], Krishna Neaupane [b], David P. Connolly [a]

[a] School of Earth and Environment, University of Leeds, Leeds, LS2 9JT, UK
[b] AECOM Ltd., Chesterfield, S41 7SL, UK

ARTICLE INFO

Article history:
Received 31 March 2022
Received in revised form
4 July 2022
Accepted 15 September 2022
Available online 28 September 2022

Keywords:
Resonance
Jointed rocks
Finite difference method
Discrete element
Transfer functions
Wave propagation

ABSTRACT

Resonance effects in parallel jointed rocks subject to stress waves are investigated using transfer functions, derived from signals generated through numerical modelling. Resonance is important for a range of engineering situations as it identifies the frequency of waves which will be favourably transmitted. Two different numerical methods are used for this study, adopting the finite difference method and the combined discrete element-finite difference method. The numerical models are validated by replicating results from previous studies. The two methods are found to behave similarly and show the same resonance effects; one operating at low frequency and the other operating at relatively high frequency. These resonance effects are interpreted in terms of simple physical systems and analytical equations are derived to predict the resonant frequencies of complex rock masses. Low frequency resonance is shown to be generated by a system synonymous with masses between springs, described as spring resonance, with an equal number of resonant frequencies as the number of blocks. High frequency resonance is generated through superposition of multiple reflected waves developing standing waves within intact blocks, described as superposition resonance. While resonance through superposition has previously been identified, resonance based on masses between springs has not been previously identified in jointed rocks. The findings of this study have implications for future analysis of multiple jointed rock masses, showing that a wave travelling through such materials can induce other modes of propagation of waves, i.e. spring resonance.

1. Introduction

Stress waves propagating through a medium are modified by the properties of that medium. If the medium is a rock mass, these properties can include the intact blocks, joints between blocks, spacing of joints and the properties of the wave itself. The intact block properties dictate the velocity at which the propagating wave travels; the joint, intact block and wave properties dictate the degree of reflection and transmission of waves from the joints (Pyrak-Nolte et al., 1990a; Cai and Zhao, 2000). The joint spacing influences how many joints there are and so the number of individual reflections which can occur in a given volume of rock. As a stress wave propagates through a jointed rock mass, the wave can have its frequencies filtered, with joints acting similarly to a low pass filter. Typically, high frequencies are filtered to a greater degree than low frequencies, although this is not always the case in multiple jointed rock masses. If certain frequencies maintain higher transmissions than those around them through interaction with the joints within the rock mass, these could be considered as resonant frequencies for the rock mass. Eitzenberger (2012) highlighted that resonance phenomena could be present in jointed rock masses excited by dynamic loads; however, this concept was not examined. Resonance is important to a range of engineering situations, such as rail engineering (Yau, 2001; Hanson et al., 2012), seismic engineering (Flores et al., 1987; Mucciarelli et al., 2004; Ariga et al., 2006), and resonance enhanced drilling (Li et al., 2019), among others. A more detailed understanding of what influences resonance in jointed rock masses can aid in the accurate prediction of potentially highly transmitted stress waves, potentially allowing these to be mitigated

* Corresponding author.
E-mail address: ee15hth@leeds.ac.uk (H. Holmes).
Peer review under responsibility of Institute of Rock and Soil Mechanics, Chinese Academy of Sciences.

https://doi.org/10.1016/j.jrmge.2022.09.001

early on in the design stage of a project. Transfer functions have the ability to capture such effects by giving the ratio of the amplitudes of an input signal to an output signal for a range of frequencies.

Stress waves interacting with joints in rock masses are a well-studied aspect of rock mechanics, with analytical, numerical and physical techniques having been used to study these problems (Schoenberg, 1980; Pyrak-Nolte et al., 1990a, b; Cai and Zhao, 2000; Zhao et al., 2006a, b, 2008; Hildyard, 2007; Barbosa et al., 2019; Zheng et al., 2020; Fan et al., 2022; Wang et al., 2022; Xu et al., 2022). Arguably, the simplest jointed problem is a planar wave normally incident on a single planar joint with elastic material properties. This case was investigated analytically by Schoenberg (1980) and later validated using laboratory scale physical models by Pyrak-Nolte et al. (1990a) giving closed form analytical expressions for the reflection and transmission of shear and compressional waves from fractures, given by Eqs. (1) and (2). These expressions give the reflection (R_1) and transmission (T_1) coefficients, defined as a ratio of the amplitude of the input to output signal, in terms of the joint specific stiffness (k), seismic impedance of the blocks on either side of the joints (z) and the angular frequency of the wave (ω), where i is $\sqrt{-1}$. These equations show that increasing k increases transmission and reduces reflection, while increasing the z or ω reduces transmission and increases reflection.

$$T_1 = \frac{2\frac{k}{z\omega}}{2\frac{k}{z\omega} - \mathrm{i}} \tag{1}$$

$$R_1 = \frac{i}{2\frac{k}{z\omega} - \mathrm{i}} \tag{2}$$

The single joint analytical functions of Pyrak-Nolte et al. (1990a) and Schoenberg (1980) have been found to behave well compared to the theory of the method of potentials (Cai and Zhao, 2000), the virtual wave source method (Zhu et al., 2011) as well as numerous numerical models (Zhao et al., 2006b, 2008; Deng et al., 2012; Zhang et al., 2019).

In most realistic situations, stress waves will encounter multiple joints as they propagate through a rock mass. These more complex, multi-joint cases have been investigated using the same techniques as adopted for single jointed conditions. Pyrak-Nolte et al. (1990b) used a laboratory experiment with a block composed of a stack of equal thickness, identical, metal plates, which behaved as a parallel jointed, homogenous rock mass. It was proposed that the transmission coefficient for the rock mass (T_N) could be approximated by the single joint transmission coefficient raised to the power of the number of joints (N), using Eq. (3). Other analytical equations have been defined for multiple parallel jointed rocks including Zhao et al. (2006b) and Li et al. (2012).

$$|T_N| = |T_1|^N \tag{3}$$

Hildyard (2007) replicated the study of Pyrak-Nolte et al. (1990b) using a numerical model solved using the finite difference method with joints modelled as displacement discontinuity elements. It was found that the waveforms from numerical modelling only matched the results from the physical model when fractures are aligned parallel to the direction of wave propagation. However, it was found that a closer match for perpendicular fractures, in relation to the wave propagation, was achieved when a stress dependent material model was adopted.

Numerical modelling studies further investigated multi jointed cases, showing that Eq. (3) only gives an approximation of the transmission coefficient. Cai and Zhao (2000) found that when there are multiple parallel joints, it is possible for a transmission coefficient to increase at certain dimensionless joint spacing ($\xi = s/\lambda$, where s is the joint spacing, and λ is the wavelength). It was proposed that this was the effect of superposition between multiple reflected and incident waves within the jointed rock mass. Multiple waves, travelling in different directions, can constructively interfere at certain frequencies, increasing the transmission coefficient, and destructively interfere at other frequencies, reducing the transmission coefficient. A similar study was conducted by Zhao et al. (2006b) with similar conclusions, proposing that an equivalent medium method could be used when the wavelength is much larger than the joint spacing. Parastatidis et al. (2017) further investigated the applicability of using an equivalent medium by modelling localised effective continua in the region of joints and comparing the results to explicitly modelled joints and a homogenous equivalent medium. It was found that a localised effective continuum model gave a better approximation of the transmitted waveform than a homogenous medium with anisotropic material properties. Considering transmission coefficients, Zhao et al. (2006b) also found that there was a zone of relatively high transmission coefficients when ξ is at a critical value, typically between 0.1 and 0.3, as found by Cai and Zhao (2000).

Most studies have considered transmission and reflection coefficients of rock masses and joints, as opposed to resonance (Pyrak-Nolte et al., 1990a, b; Cai and Zhao, 2000; Zhao et al., 2006b). When the transmission at a particular frequency is higher than surrounding frequencies, a resonant frequency for the rock mass has been identified. It could be argued that Cai and Zhao (2000) and Zhao et al. (2006b) identified resonance in their models, but in terms of ξ. Resonance is an important consideration in many engineering studies, not least railway engineering. Resonance in buildings and the track structure are known to accentuate vibration problems (Yau, 2001; Hanson et al., 2012; Connolly et al., 2016). Resonance effects in rocks were explicitly studied by Li et al. (2019) who used a three-dimensional (3D) finite element model to study the resonance of different sized and shaped intact blocks using different excitation frequencies, with resonance depending on the block properties and dimensions. The reasons behind why such frequencies were resonant were not well defined in the study. The resonant frequencies in the study varied in a systematic manner when the block size increased, which indicates that the resonance may be due to the superposition of the incident wave and a reflected wave from the edge of the modelled block. A standing wave could develop with the incident and reflected waves, causing wave superposition and an increase in the transmission coefficient. The outcomes of the study by Li et al. (2019) and Zhao et al. (2006b) appear to differ, with the former identifying superposition at much higher frequencies than the latter. Resonance from the superposition of reflected waves has been identified by Nakagawa (1998), who gave analytical equations for resonance, terming it acoustic resonance. Acoustic resonance in natural stone blocks is a reasonably well established effect, being the subject of a British national standard (BS EN 14146:2004, 2004).

There appear to be overlapping effects occurring in regard to stress wave transmission through jointed rock masses that have been identified in the literature, although up to this point full transfer functions have not been generally used in the analysis of jointed rock masses. This study explores the effects that different jointed rock masses can have on a rock mass transfer function using both the finite difference and combined discrete element-finite difference modelling methods. Despite these numerical methods being used previously (Cai and Zhao, 2000; Zhao et al., 2006b; Eitzenberger, 2012; Parastatidis et al., 2017), the processing of the data using the full waveform with a transfer function provides a new lens in which to view rock mass transmission. Analysing the full waveform allows a more accurate means of determining the frequencies of waves that will be transmitted to a receptor.

Mechanisms are proposed for the resonance effects identified and simple analytical models derived giving fast and accurate prediction of resonant frequencies for complex rock masses. This study's findings are interpreted in the context of previous research to understand the effects observed and further validation work is highlighted.

2. Methodology

Two different numerical modelling techniques are used in this study. A one-dimensional (1D) combined finite difference-discrete element model, as used by Cai and Zhao (2000), Zhao et al. (2006b) and Eitzenberger (2012), and a two-dimensional (2D) finite difference model, as used by Parastatidis et al. (2017) are created, solved in the universal discrete element code (UDEC) (Itasca, 2014) and WAVE2D (Hildyard et al., 1995), respectively. Two different numerical models are used as a first step in verification of the results.

A 500 Hz signal frequency is used as the excitation source for both models; however, different wave forms are generated, with a Gaussian wave in UDEC and a modified Ricker wave in WAVE2D, both shown in Fig. 1. As a transfer function method is adopted, the difference in waveform will not present any issues when comparing the results from the models.

No material damping is modelled and the plane wave fills the full model height in both UDEC and WAVE2D, preventing any geometrical damping. Therefore, there should be no decay of the wave signal through the model and any modifications to the wave will be caused by interaction with joints. The velocity responses of the models are recorded before the joints, close to the excitation source, and after the joints. This gives input and response waveforms from the model.

There are differences in the way the models treat joints and blocks, the waveforms used for the excitation and the mesh sizes used for each model. For instance, the frequency contents of the wave in the two models are not exactly the same, as shown in Fig. 1. The treatment of the blocks and joints and mesh sizes are described in the following sections. These differences will highlight possible modelling artefacts as well as giving results that are more robust.

2.1. UDEC model description

UDEC, using the combined finite difference-discrete element method, treats individual blocks as discrete elements with joints being the interface properties between each of the blocks (Itasca, 2014). Joints in UDEC split the model up into blocks, which are allowed to undergo significant degrees of movement. The blocks are discretised using a finite difference mesh composed of quadrilateral elements, allowing deformations of the blocks. Fractures within the model are treated as block interfaces, which behave as linear-elastic displacement discontinuities.

A 1D model is generated, which is achieved in the 2D software by only allowing the finite difference mesh to generate one node in the out of plane direction (Fig. 2). The horizontal boundaries are modelled as being fixed for velocity in the vertical direction, but free in the horizontal direction, meaning that the single zone can only move in one direction; therefore, making the model effectively 1D. The plane wave is induced at the left hand model boundary as a horizontal force function. This generates a compressional stress wave, which propagates along the model from left to right (Fig. 2). The vertical model boundaries are sited at a large distance from the joints to prevent reflections from the model boundaries polluting the signal. Despite this, the vertical boundaries are modelled as absorbing boundaries, using a horizontal dashpot with material properties of the intact rock, to reduce the risk of reflections.

All models used to generate the results in Section 3 have a P-wave velocity (C_p) of 3328 m/s. Therefore, with a mesh size of 0.125 m, and observing the rule of wavelength needing to be greater than 10 times the mesh size (Cai and Zhao, 2000), the

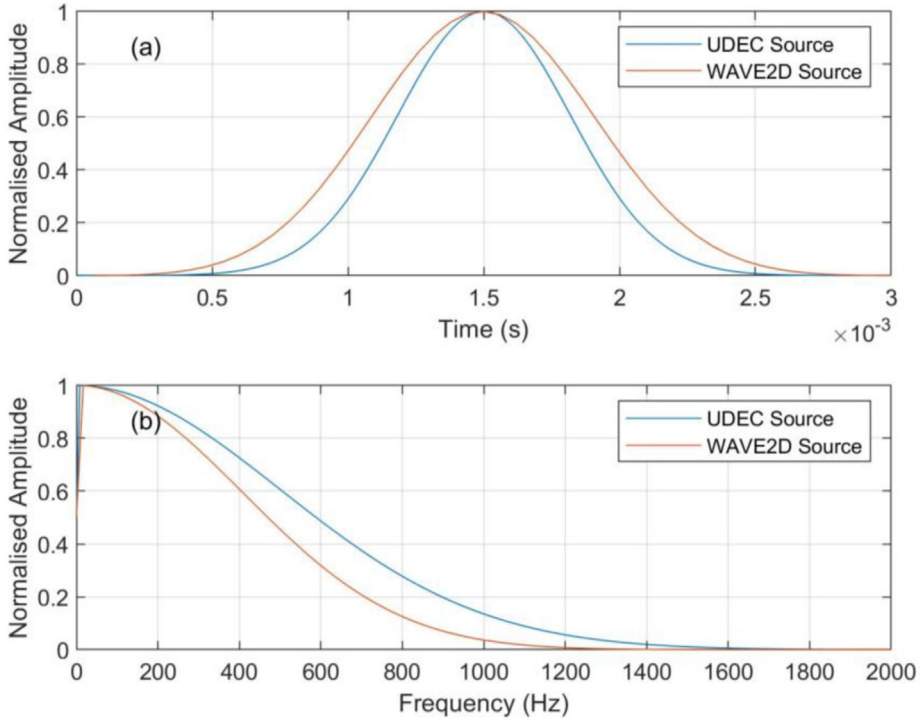

Fig. 1. Input waves to UDEC and WAVE2D models: (a) Time series of sources, and (b) Frequency content of sources. UDEC is a 500 Hz Gaussian wave and WAVE2D is a 500 Hz modified Ricker wave.

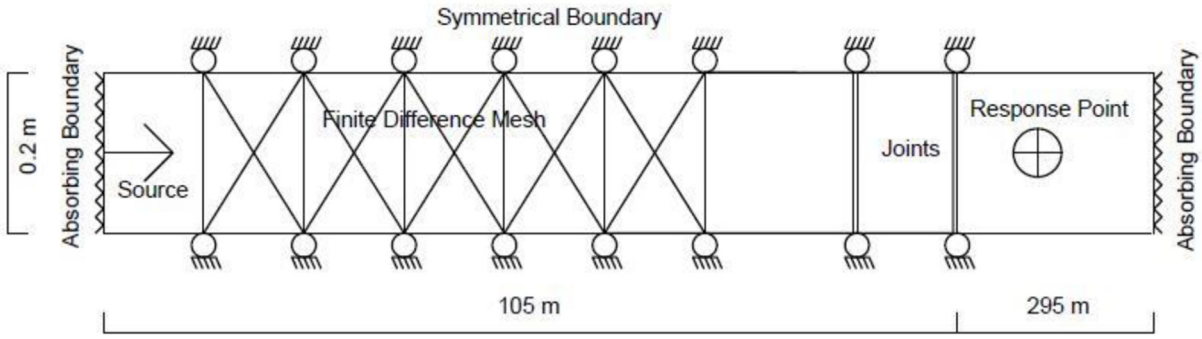

Fig. 2. UDEC model showing finite difference mesh. Mesh fills entire model. Not to scale.

models will be able to accurately transmit frequencies up to 2662 Hz. This is greater than the frequency range of the wave source applied to the UDEC model, as shown in Fig. 1.

2.2. WAVE2D model description

WAVE2D handles joints as special displacement discontinuity elements within the model (Hildyard et al., 1995). These are given the same properties as the block-block interfaces in UDEC; however, the blocks are not separate entities as they are in UDEC. The joints are implemented in the mesh as two infinitesimally thin planes and employing fictional stresses within the joint. A detailed derivation of the joint deformation equations are given by Hildyard et al. (1995).

A 2D model is used in WAVE2D with a plane wave induced across the entire short axis of the model, which propagates along the long axis. Although this model is 2D, the application of the plane wave causes the model to behave as though it is 1D. This is much like the pseudo-1D set up used by Cai and Zhao (2000). The excitation is generated as a horizontal velocity function, generating a compressional wave, which propagates from left to right. The excitation source is located 0.8 m from the left-hand vertical boundary. The source cannot be applied exactly on the boundary in WAVE2D; however, the source has been applied as close to the boundary as it can be, to give a similar modelling scenario as that modelled in UDEC. A square mesh of finite difference quadrilaterals is created, with edge lengths of 0.08 m. There are 4800 elements in the long axis and 2080 elements in the short axis (Fig. 3), giving dimensions of 384 m horizontally and 166.4 m vertically.

The vertical boundaries are modelled as absorbing with the horizontal boundaries, orientated perpendicular to the wave propagation direction, as plane wave boundaries.

The intact block properties of the WAVE2D models are the same as those applied to the UDEC models, with a C_p of 3328 m/s. Given the mesh size of 0.08 m, the models described here will be able to accurately transmit waves up to 4160 Hz, which is much greater than the frequency range of the source wave shown in Fig. 1.

2.3. Transfer functions

The numerical tools used for this study have been used for similar problems (Cai and Zhao, 2000; Zhao et al., 2006a; Parastatidis et al., 2017). The innovation in this study is to design the models such that transfer functions can be extracted which produces results across a broad band of frequencies through analysis of the full waveforms. Non-normalised material properties are preferred for the relationships identified in this study. Despite normalised stiffness and wave terms being used extensively in studies of transmission of stress waves through joints (Cai and Zhao, 2000; Zhao et al., 2006b; Li et al., 2012; Zheng et al., 2020; Xu et al., 2022, among many others), normalised terms hinder the use of transmission relationships with other areas of engineering. These tend to give vibration sources in terms of absolute frequency, such as high-speed rail (Connolly et al., 2016). Therefore, the relationships defined in this study can be easily applied across engineering disciplines.

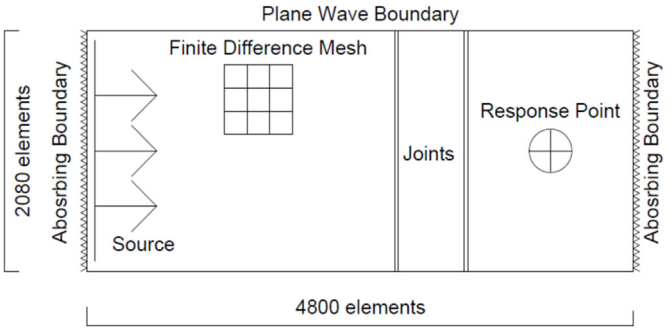

Fig. 3. WAVE2D model showing finite difference mesh. Mesh fills entire model. Not to scale.

Transfer functions describe the difference between the magnitude of the frequencies of two signals, such as a source and a response. In this study, the signals are recorded as velocity-time series at the source (signal) and some distance from the source (response). To generate a transfer function, the time series are decomposed into their harmonic components and the discrete frequencies in the signal and response are compared. If the amplitude of the signal and response at a given frequency are the same, the transfer function for that frequency will be equal to 1. If the response has an amplitude of half the source, the transfer function for that frequency will be 0.5, and if the response has an amplitude twice the source, the transfer function for that frequency will be 2. Transfer functions represent a convenient method for determining how a medium affects a propagating wave, regardless of the amplitude and waveform of the input signal.

An example of the procedure of generating a transfer function is shown in Fig. 4. The UDEC model shown in Fig. 2 was modelled without joints and the source and response of the model recorded. This also serves as a calibration case to show that the model is performing as expected. As there is no material damping and the model is 1D, eliminating geometrical damping, the wave will not be altered as it passes through the model. The time series of the source and response are plotted in Fig. 4a. The transfer function for these two time series is plotted in Fig. 4b, which is shown to be equal to 1 at all frequencies.

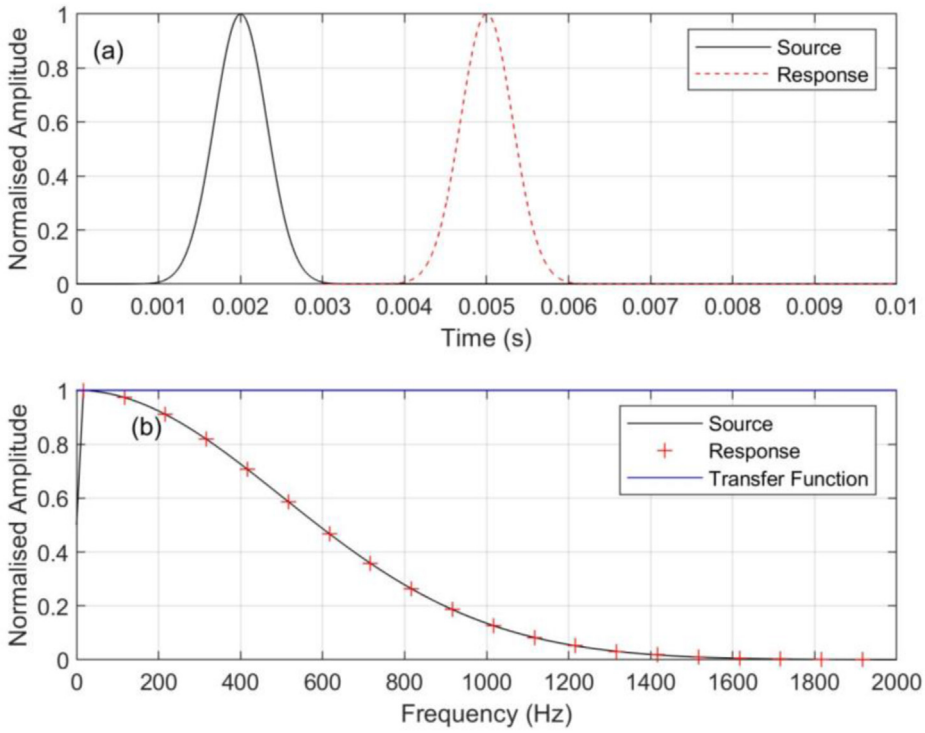

Fig. 4. Example of a transfer function derived from a time series in an unjointed and undamped 1D UDEC model with a C_p of 3328 m/s and mesh size of 0.125 m: (a) Time series of source and response, and (b) Frequency content of source and response and transfer function.

3. Results

Modelling is undertaken in both UDEC and WAVE2D using the models shown in Figs. 2 and 3, with more joints added when required. To generate the database used for the analysis in this study, a wide range of models were considered. Models in the study have joint numbers (J_n) of 2–8, C_p of 2365–5910 m/s, Young's modulus (E) of 11.1–88.3 GPa, joint spacing (s) of 1–8 m and material densities (ρ) of 260–26,000 kg/m^3. For brevity, not all results are included here, although a sample of the data is shown in Table 1, with additional results included in Appendix A. All models have a mesh size of 10 times the minimum wavelength, up to a frequency of at least 1800 Hz.

The transfer functions for the models included in Table 1 are shown in Figs. 5–7. The figures show that some frequencies are transmitted through the joints with a greater transmission coefficient than others. Each transfer function shows that there are three main bands with high transmission: very low frequency, low frequency and high frequency. All of the models show a transmission coefficient of 1 as the frequency approaches 0 Hz. This high transmission at very low frequencies is not included in the results in Table 1 as this is a consequence of a very low frequency wave passing through the model unhindered by joints, as predicted by Eq. (1). All models show a second peak at low frequencies, before an area of low transmission. This low frequency resonant peak appears to move significantly as the density and joint specific stiffness of the model change. For a high density block with a low joint specific stiffness, as shown in Fig. 5a, the resonant frequency is less than 50 Hz, while for the same density model with a high joint specific stiffness, as shown in Fig. 5c, the resonant frequency is at 100 Hz. In the low density model with a low joint specific stiffness, as shown in Fig. 7a, the resonant frequency is at 250 Hz, while the same model with a high joint specific stiffness, as shown in Fig. 7c, the resonant frequency is at 500 Hz. These both show a doubling of the resonant frequency while the joint specific stiffness increases by an order of magnitude, form 1 GPa/m to 10 GPa/m.

UDEC tends to show a slightly lower resonant frequency than the equivalent WAVE2D models. The reason behind this is the subtly different geometries used in UDEC and WAVE2D. Despite the symmetrical boundaries applied to the UDEC model, the single element in the out of plane direction means the models behave slightly differently.

The high frequency resonant peak does not move significantly as the model properties change, although there are small variations, with a greater variation occurring when the model has a low stiffness, compared to a high stiffness. For instance, Fig. 5b and c shows a high frequency resonant peak at approximately 830 Hz, with joint specific stiffnesses of 4 GPa/m and 10 GPa/m, respectively. The lowest joint specific stiffness, in Fig. 5a, does not show a

Table 1
Models used in sensitivity analysis in UDEC and WAVE with their resonant frequencies.

ρ (kg/m^3)	C_p (m/s)	C_s (m/s)	E (GPa)	k_n (GPa/m)	s (m)	J_n	Resonant frequency (Hz)			
							UDEC		WAVE2D	
							1st	2nd	1st	2nd
26,000	3328	1922	240	1	2	2	28	–	32	–
26,000	3328	1922	240	4	2	2	56	835	61	830
26,000	3328	1922	240	10	2	2	87	841	96	843
2600	3328	1922	24	1	2	2	87	840	96	845
2600	3328	1922	24	4	2	2	162	867	187	877
2600	3328	1922	24	10	2	2	235	914	250	932
260	3328	1922	2.4	1	2	2	237	914	250	932
260	3328	1922	2.4	4	2	2	342	1052	369	1082
260	3328	1922	2.4	10	2	2	387	1144	425	1165

Note: C_s denotes the shear wave velocity, k_n denotes the joint normal specific stiffness, and '-' denotes no results visible in model.

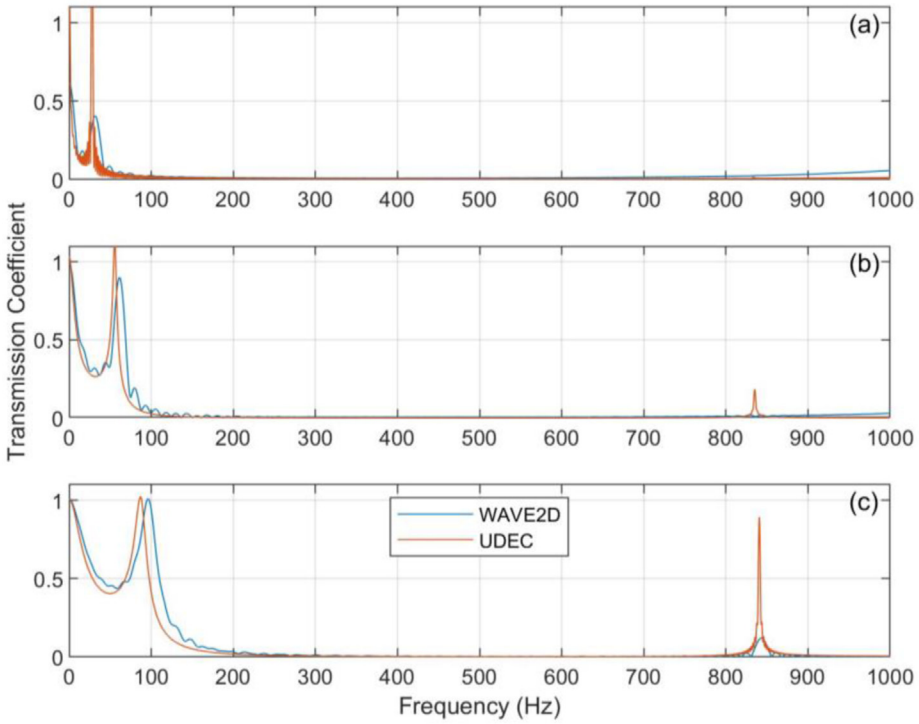

Fig. 5. High density (26,000 kg/m^3) transfer functions from WAVE2D and UDEC for a material with C_p of 3328 m/s and C_s of 1922 m/s: (a) $k_n = 1$ GPa/m, (b) $k_n = 4$ GPa/m, and (c) $k_n = 10$ GPa/m.

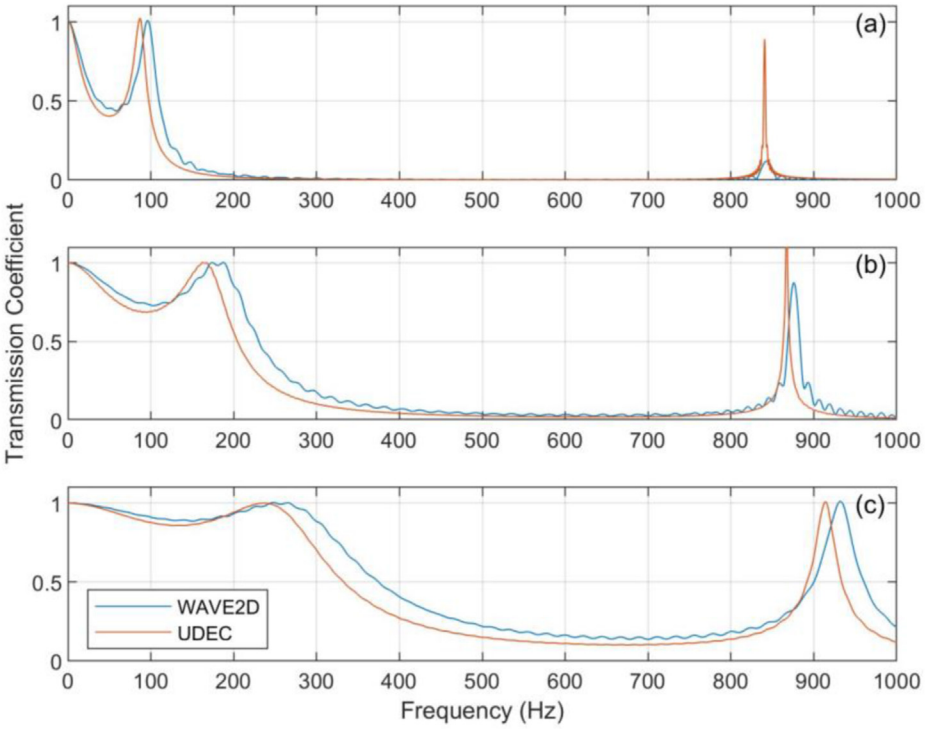

Fig. 6. Medium density (2600 kg/m^3) transfer functions from WAVE2D and UDEC for a material with C_p of 3328 m/s and C_s of 1922 m/s: (a) $k_n = 1$ GPa/m, (b) $k_n = 4$ GPa/m, and (c) $k_n = 10$ GPa/m.

high frequency resonance. As these are from a model with a high density, the elastic stiffness of the model will also be high when compared to a model with the same velocity but a lower density, as shown in Fig. 6. In Fig. 6a, the high frequency resonance is at 830 Hz, moving to 870 Hz in Fig. 6b and to 930 Hz in Fig. 6c. These show an increase in the joint specific stiffness from 1 GPa/m to

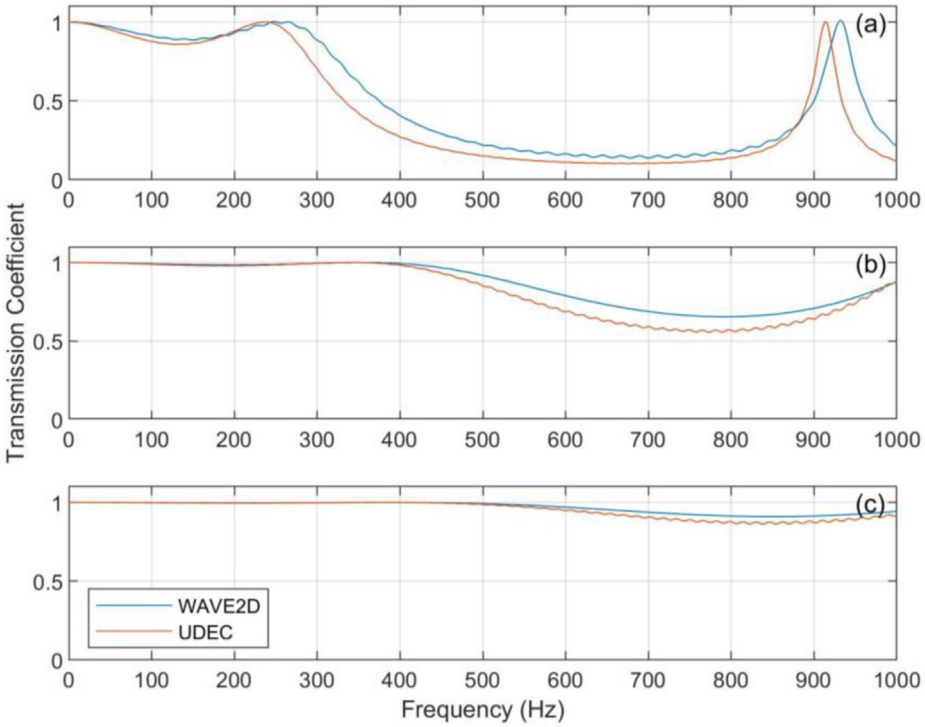

Fig. 7. Low density (260 kg/m^3) transfer functions from WAVE2D and UDEC for a material with C_p of 3328 m/s and C_s of 1922 m/s: (a) k_n = 1 GPa/m, (b) k_n = 4 GPa/m, and (c) k_n = 10 GPa/m.

10 GPa/m, which corroborate the qualitative remark made at the start of this paragraph.

Some of the transmission coefficients, especially in the UDEC models, reach a transmission coefficient greater than 1. This implies that there is more energy at this frequency than was input to the model; however, it is also possible that it is caused by noise in the data generating an artificially high peak. Despite this, some trends can be observed in the relative magnitude of the transmission coefficients. The amplitude of the lower density models, as shown in Fig. 7, is higher than that of the higher density models, as shown in Fig. 5. Therefore, it can be said that the joints in the lower density models do not hinder the transmission of stress waves as much as joints in the higher density models, which act to filter out certain frequencies. This is likely to be due to the joints in the lower density, and therefore lower stiffness, models being stronger than, or more similar to, the stiffness of the intact block material. Therefore, these joints will not affect the waves as much as lower stiffness joints. Some filtering effects would be expected as the joints do not have an infinite stiffness, which is required for a welded interface. The logical progression of this is that, for the same range of joint specific stiffness used in Table 1, as the stiffness of the models increases, the amplitude of the transfer function would reduce, with this being more evident at higher frequencies. This can be seen in Fig. 5a, where the high frequency resonance, which should be somewhere near 800 Hz, is not visible in either model. The lower stiffness models have a much less obvious low frequency resonant peak, which occurs at a much higher frequency, when compared to the higher stiffness models, where the low frequency resonance is clear.

When additional data are studied, as shown in Appendix A, further trends become apparent. The number of low frequency peaks increases as the number of joints increases. Appendix A shows that the number of low frequency resonant peaks is equal to J_n-1. This effect is also shown in Fig. 8, with J_n of 2, 3 and 5 (not all included in Appendix A), with the data generated from UDEC. The frequency of the low frequency resonance does not appear to relate to the C_p, as when k_n, J_n and s are kept constant and C_p changes this peak does not move significantly.

The frequency of the high frequency peaks appears to be related to the wavelength of the wave. The first peak always has a wavelength twice the joint spacing, the second a wavelength equal to the joint spacing, the third a wavelength two thirds of the joint spacing and the fourth a wavelength of half the joint spacing. Fig. 8 shows that there can be an equivalent number of peaks making up the high frequency peak as there are low frequency peaks, although these tend to be very close together and are treated as a single peak in this study. The frequencies of these peaks are mainly influenced by the s and C_p, and not greatly by k_n. As the material stiffness changes, due to the change in C_p, and k_n increases, the first peak diverges from having a wavelength equal to 2s. A low k_n and relatively high material stiffness appear to fit the trends most precisely.

4. Analytical expressions

It is postulated that the observed resonances result from two separate physical mechanisms, i.e. a mass-spring resonance and a superposition resonance. Therefore, attempts are made to derive analytical expressions for the frequencies of these resonances based on these two mechanisms.

4.1. Low frequency resonance – spring resonance

The low frequency resonance seems to show complex trends, with the number of resonant frequencies increasing when the number of joints increases (Fig. 8) and their frequency related to the properties of the blocks and joints (Figs. 5–7). In order to explore the trends in the data, it is beneficial to be able to link these to simple physical cases with closed form solutions. To do this,

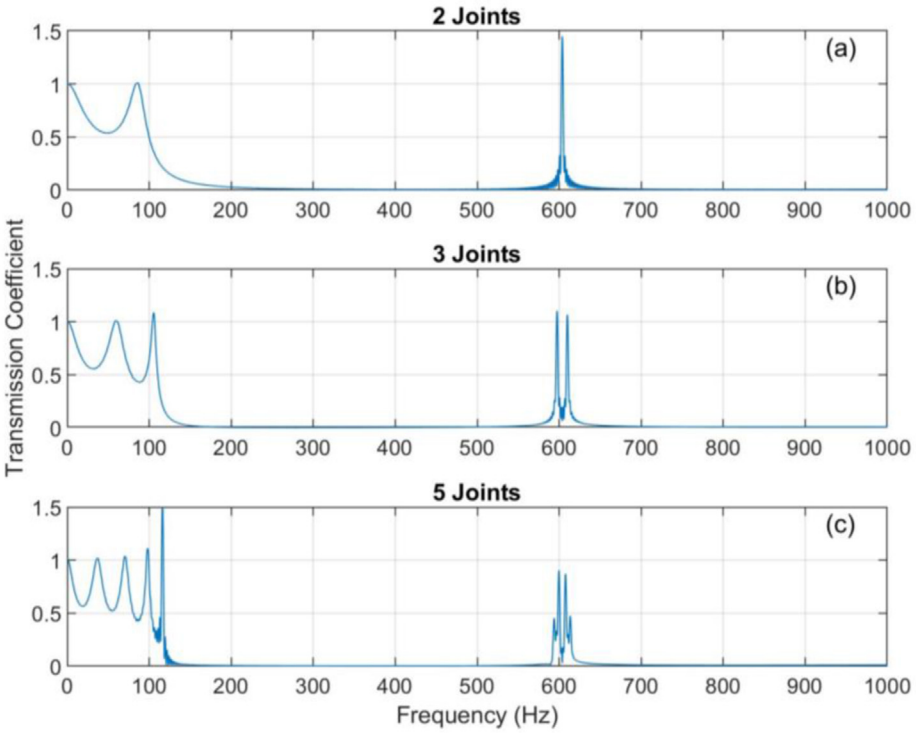

Fig. 8. Transfer functions for identical rock masses ($s = 2$ m, $C_p = 2365$ m/s, $C_s = 1922$ m/s, $k_n = 1$ GPa/m, $\rho = 2600$ kg/m^3) with different numbers of joints: (a) 2 joints, (b) 3 joints, and (c) 5 joints.

initially, the simplest jointing case of two parallel joints will be explored.

A model with two parallel joints is equivalent to a block between two springs which are fixed at their ends (Fig. 9). The block is created by the joints, with the joints operating like springs. The large blocks on either side of the joint generated block (Figs. 2 and 3) operate to fix the springs (joints) in position. This is not strictly accurate as these end blocks can deform; however, for the purposes of a simple analogy, this system will suffice. In the 1D models used here, the mass can only move in a single plane. The block will oscillate at a frequency related to the stiffness of the springs and the mass of the block. Eq. (4) gives the frequency of oscillation of a mass between two springs.

$$\omega = \sqrt{\frac{2K}{m}} \tag{4}$$

where m is the mass of the block, and K is the stiffness of the springs.

Eq. (4) can be used with different stiffnesses on either side of the block, in which case $2K$ would become $K_1 + K_2$, with K_1 and K_2 being the different spring stiffnesses. The m is given by the block density multiplied by the joint spacing ($m = s\rho$).

To extend this analogy to more complex rock masses, additional blocks and springs can be added. When there are more blocks added, more resonant frequencies are generated, with the same number of resonant frequencies as the number of blocks. Earlier it was highlighted that there was one less low frequency resonant peak than the number of joints, which is equal to the number of blocks in the model, not including the blocks in contact with the ends of the model. The ω of the resonant peaks are given by the eigenvalues (α) of Eq. (5).

$$\boldsymbol{K}_m\boldsymbol{X} = \alpha\boldsymbol{M}\boldsymbol{X} \tag{5}$$

Fig. 9. A single degree of freedom mass between two springs used as an analogy for a parallel jointed rock mass.

$\boldsymbol{K}_m$ is the stiffness matrix (Eq. (6)) and $\boldsymbol{M}$ is the mass matrix (Eq. (7)):

$$K_m = \begin{bmatrix} k_1 + k_2 & -k_2 & \cdots & 0 \\ -k_2 & k_2 + k_3 & \ddots & \vdots \\ \vdots & \ddots & \ddots & -k_j \\ 0 & \cdots & -k_j & k_{j-1} + k_j \end{bmatrix} \tag{6}$$

$$M = \begin{bmatrix} m_1 & 0 & \cdots & 0 \\ 0 & m_2 & \ddots & \vdots \\ \vdots & \ddots & \ddots & 0 \\ 0 & \cdots & 0 & m_j \end{bmatrix} \tag{7}$$

where m_j is the jth block mass, k_j is the jth spring stiffness, and $\boldsymbol{X}$ is a vector that satisfies Eq. (5).

Eq. (5) does not give the exact answer given by the numerical models. The difference suggests that the numerical models are not quite behaving like a rigid mass between two springs. The finite difference method, in its essence, attaches a number of springs in series, especially when modelled as a 1D material, as is the case here. There are springs for the intact material with one stiffness, attached to springs for the joints of another stiffness, again attached

to springs for the intact material, and so on. As the blocks are able to accommodate deformations, not just the joints, the deformation of the blocks could be changing the effective stiffness of the material. The stiffness for a jointed rock mass can be calculated as the static stiffness of a series of springs, using Eq. (8) (Ma et al., 2013), which can be incorporated into Eq. (6) to account for the deformability of the blocks.

$$K_c = \frac{1}{\frac{1}{E_i} + \frac{1}{k_n}} \tag{8}$$

where K_c is the combined spring stiffness, and E_i is the intact block Young's modulus.

Using K_c, calculated from Eq. (8), as the spring stiffness (k_j) in Eq. (6), the predicted resonant frequency reduces, bringing it closer to the numerical modelling results, although they are still not exactly the same. There is also a difference in the error associated with the two numerical models, with UDEC having a greater error than WAVE2D. The reason behind this being the slightly different geometries of the two models, meaning they are analysing to different problems. Despite the disagreement between the exact resonant frequency of the two numerical models, even for the simple cases given here, the spring effects displayed by the models are clear.

A final equation for the prediction of the low frequency resonant frequencies is given by Eq. (9), and in terms of the ξ, by Eq. (10). The term low frequency resonance is quite ambiguous, thus this effect will be referred to from now on as spring resonance.

$$f_n = \frac{1}{2\pi}\sqrt{\alpha_n} \tag{9}$$

$$\xi = \frac{s}{2\pi C_p}\sqrt{\alpha_n} \tag{10}$$

where f_n is the nth resonant frequency, α_n is the nth eigenvalue for the system, and n is the peak number which has values from 1 to J_n-1.

Spring resonance is considered to be applicable for all rock masses which show linear elastic joint behaviour, and is not limited to the range of properties shown in Table 1 or Appendix A.

4.2. High frequency resonance – superposition resonance

The wavelengths of the high frequency resonance appear to be closely related to the joint spacing. The relationships in terms of ξ are shown in Table 2. The peaks are numbered following on from the resonances generated through spring resonance, of which there are J_n-1 resonances. The frequency that gives these wavelengths can be calculated from Eq. (11), with Eq. (12) giving the same equation in terms of ξ. This equation is the same form as the classical equation which gives the frequencies which generate a standing wave on a string fixed at its ends, of length s, and has been found to give rock resonance by Nakagawa (1998). Using the standing wave analogy, the string is the equivalent of a block and the fixed ends are equivalent to the ends of the block, or joints. Multiple reflected waves, travelling in opposite directions, can superimpose, amplifying the transmitted wave. Therefore, a wave of these wavelengths will have a greater transmission coefficient than a wave of a higher or lower frequency. The length of s has no physical limits, although in numerical modelling, it will be limited to a maximum of the size of the model and a minimum of 10 times the mesh size.

Table 2
Wavelengths as a multiple of joint spacing for high frequency resonance in jointed rock masses.

Peak number, n	ξ
J_n	0.5
$J_n + 1$	1
$J_n + 2$	1.5
$J_n + 3$	2

$$f_n = \frac{(n - J_n - 1)C_p}{2s} \tag{11}$$

$$\xi = \frac{n - J_n - 1}{2} \tag{12}$$

where n is the peak number, including all spring resonance peaks.

This high frequency resonance will be referred to as superposition resonance from now on, to avoid ambiguity in the term.

Eq. (11) does not give the exact resonant frequency and instead serves as a reasonable estimate. The reasons behind this are likely to be due to the deformation of the blocks during the analysis, therefore changing the size of the blocks and the frequencies which can form standing waves within them. This assumption is supported when viewing different block and joint stiffnesses. The stiffness of the blocks appears to significantly affect the resonant frequency, as shown in Table 1, with the very low stiffness blocks diverging significantly from the frequency predicted by Eq. (11). The resonant frequency from modelling increases as the intact material stiffness decreases, giving a lower wavelength. A lower material stiffness will allow the block to deform more; therefore, allowing compression, reducing the size of the block. Increasing k_n also increases the frequency, further reducing the wavelength. A stiffer joint will deform less; therefore, causing all deformation to be focussed in the block, further reducing the block size and reducing the wavelength. These effects are only evident in very low stiffness materials with very high stiffness joints, which are not likely in reality. In most realistic rock masses, Eq. (11) would be expected to give a reasonable approximation of the resonant frequency.

Theoretically, there are an unlimited number of superposition resonant frequencies. However, as shown in Fig. 5, the high frequency resonance may not be visible for low stiffness joints. This is likely to be related to the effects shown by the single joint analytical equations (Eqs. (1) and (2)) (Schoenberg, 1980; Pyrak-Nolte et al., 1990a). A combination of a very low stiffness joint and a high material stiffness will prevent energy from being transmitted. Despite this generating a large degree of reflection to allow the superposition, if energy cannot be transmitted through the joint, there will be no increase in transmission on the other side of the joints. Eq. (1) shows that the degree of transmission also reduces as the frequency increases, hence this implies that as the order of the superposition peak increases, which increases the frequency, its magnitude will decrease. Fig. 10 shows the results of a model with a wide joint spacing, in order to generate a large number of superposition resonant frequencies. This clearly shows that as the superposition resonant frequency increases, the amplitude of this peak reduces. The absolute amplitude of the resonances may be incorrect due to noise in the data, although it is clear that the relative amplitude of the peaks reduces as the frequency increases.

4.3. Verification of the resonance mechanisms

The mechanisms identified in the transfer functions are verified using a numerical model excited by harmonic waves at a single frequency. The frequency of the excitation will be changed with the response of the model recorded, giving a frequency sweep experiment. The rationale behind this experiment is that when a resonant frequency is applied, the numerical model will show a greater response than when a non-resonant frequency is applied to the model. The response recorded will be the peak particle velocity (PPV) after the joints. The model set up is identical to the UDEC model in Fig. 2, with the following properties: $J_n = 3$, $s = 2$ m, $k_n = 1$ GPa/m, $C_p = 3328$ m/s, $C_s = 1922$ m/s, $\rho = 2600$ kg/m^3.

The frequency sweep of the model will be conducted between 10 Hz and 1000 Hz. The resolution of the frequency sweep will be finer in the areas where resonance is predicted, given by Eqs. (9) and (11), and coarser outside of these areas. The model used here is expected to have spring resonance at 62 Hz and 107 Hz, with superposition resonance at 832 Hz. The results of this experiment are shown in Fig. 11.

In Fig. 11, the analytical resonance, numerical transfer function and numerical frequency sweep methods show the spring resonance effect at the same frequencies. These occur at the predicted frequencies of 62 Hz and 107 Hz. The frequency sweep has been targeted to find these resonances; however, the peak response of the frequency sweep is much greater than the surrounding frequencies, thus this effect is unlikely to be an effect of the experiment set up.

Superposition resonance is seen at approximately 845 Hz in the numerical frequency sweep data, which is slightly greater than the analytical frequency of 832 Hz but similar to the numerical transfer function frequency, seen at 836 Hz and 845 Hz. The peak of this is quite low, although it is clearly a localised peak compared to the data surrounding this.

There are clear differences with the response of the two numerical experiments. The transmission coefficients of the frequency sweep data are lower for the resonant frequencies, while they are greater for non-resonant frequencies. Between 200 Hz and 800 Hz, the transfer function data show a transmission coefficient of close to zero, while the frequency sweep data show a transmission coefficient of approximately 0.5. The difference here is likely to be due to the different techniques used to measure the response of the models. The transfer function sends a single excitation pulse and records the full waveform transmitted through the joints, while the frequency sweep method applies a constant harmonic excitation for the duration of the model run and records the PPV of the model, which can occur at any time. Despite the differences in the techniques used and the amplitude of the transmission coefficients, the presence of the resonant frequencies is clearly evident in the two different numerical experiments. This supports the hypothesis that the two resonance mechanisms, of spring and superposition resonances, do exist in jointed rock masses.

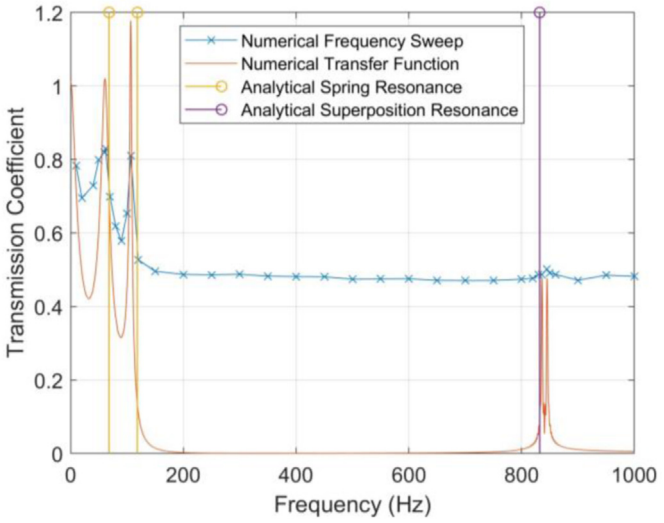

Fig. 11. Resonance mechanism verification using a numerical frequency sweep and numerical transfer function. Resonance form analytical functions is also shown. $J_n = 3$, $s = 2$ m, $k_n = 1$ GPa/m, $C_p = 3328$ m/s, $C_s = 1922$ m/s, $\rho = 2600$ kg/m^3.

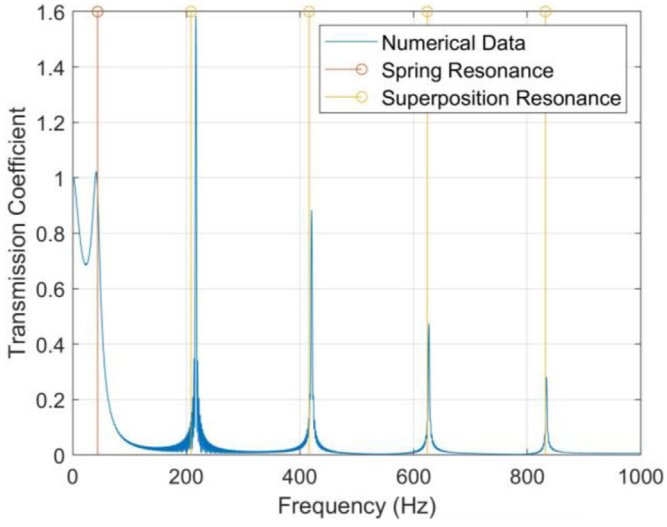

Fig. 10. Resonance shown by a jointed rock with $s = 8$ m ($C_p = 3328$ m/s, $C_s = 1922$ m/s, $\rho = 2600$ kg/m^3, $k_n = 1$ GPa/m, $J_n = 2$). Numerical data are obtained from a 1D UDEC model; spring resonance and superposition resonance are derived from Eqs. (9) and (11), respectively.

4.4. Application of analytical models

The analytical equations for spring and superposition resonances are given in terms of frequency and ξ in Eqs. 9–12. These allow a more direct comparison with previous research into multi-jointed rock masses (Cai and Zhao, 2000; Zhao et al., 2006b), using the equations in terms of ξ, and application of the results to other branches of engineering more easily, using the equations in terms of frequency. For example, the results could be applied to vibration research, such as high-speed rail, to determine whether a rock mass will preferentially transmit the frequencies generated by a vibrational source. Results from such studies are typically given in terms of frequency, instead of ξ. For example, Connolly et al. (2016) gives excitations expected from rail traffic in terms of frequencies, which can be directly compared to the results of Eqs. (9) and (11).

In order to test the analytical solutions, a series of arbitrary test cases is modelled in UDEC and WAVE2D with the resonant frequencies compared to those predicted by the analytical functions. These cases have been run in the models shown in Figs. 2 and 3. The properties of the verification cases are shown in Table 3.

(1) Case 1 contains three joints with the same stiffness, but with different joint spacings. The first and second joints are separated by 4 m and the second and third joints by 2 m.
(2) Case 2 contains two joints with different joint specific stiffnesses, where the first joint has a lower stiffness than the second.
(3) Case 3 contains two joints with different stiffnesses, where the first joint has a higher stiffness than the second.

Table 4 contains the results for Cases 1–3, solved in UDEC, WAVE2D and the analytical models. Only the first two superposition resonant peaks are shown. The analytical superposition resonant frequencies for Case 1 are calculated using both joint spacings, with the two lowest frequency peaks taken from this. In some cases, the superposition resonance is not apparent in the numerical data past the first peak, thus it is not included in the tabulated numerical results. The results in Table 4 seem to show a reasonable agreement between the numerical and analytical results. Cases 2 and 3 are diverse and different from the data set used to define the analytical models, hence the agreement of the results supports the hypothesis that the analytical models are performing as expected. This also adds weight to the idea that the spring and superposition mechanisms are realistic.

With the mechanisms behind the analytical models shown to occur in more complex rock masses than the simple cases used to identify the effects, and the resonance mechanisms verified using a frequency sweep approach (Fig. 11), the analytical models can be reasonably extrapolated beyond the data range used to define them. Table 5 shows the final spring and first superposition resonant frequencies for identical rock masses with different values of J_n. This shows that the final spring resonant frequency tends to a constant value as J_n increases, which is related to the properties of the rock mass. As the number of joints increases, there will be more blocks and therefore more resonant frequencies, thus the frequency spacing of the resonance will reduce. With a large number of joints, the spring resonance will resemble an increased transmission zone, rather than having the peaked effect as shown in previous figures. This is brought about by the frequency spacing of the resonant peaks reducing as the number of resonances increases, with all the resonances still being squashed into the same range. The previously clear peaks and troughs, as shown in Fig. 8, will be less clear with all the peaks merging into, effectively, a single wide peak. For instance, the 10,000 resonant peaks for the rock mass in the final row in Table 5 would have an average spacing of 0.05 Hz. While strictly speaking these could be seen in the transfer function, for any practical application, the peaks would merge. The first superposition resonant frequency is always at the same frequency, as it is generated by the superposition of waves of a particular wavelength and is unaffected by the number of joints.

5. Discussion

The preceding sections have identified two resonant frequency mechanisms in multiple jointed materials, spring and superposition resonances. These mechanisms have been shown to occur for materials with a wide range of different properties and joint spacings. Therefore, the analytical models in this study can be confidently applied to all jointed media, including natural jointed materials from the weakest of sandstones through to the strongest of granites, as well as synthetic jointed materials, such as aligned metallic or mortar blocks (Pyrak-Nolte et al., 1990b; Zhao et al., 2006a) and masonry structures.

While the superposition mechanism has been previously described (Nakagawa, 1998), the spring resonance mechanism has not been, despite being based on the simple system of masses between springs. Superposition effects are a common theme in relation to the transmission coefficient from jointed rock masses. Cai and Zhao (2000) and Zhao et al. (2006b, 2008) identify an increased transmission zone occurring when the ξ of the rock mass is very low, which was explained as a superposition effect of multiple reflected waves. Cai and Zhao (2000) found that the greatest transmission coefficient occurred with a ξ of 0.075, and an increased transmission zone between ξ of 0.05 and 0.3, with no increase in transmission at 0.5. Similar results were found by Zhao et al. (2006b, 2008) and also replicated by Xu et al. (2022). The values found by these studies are much lower than what would be expected to generate superposition resonance. The previous studies give analytical equations for the first arrivals of a sine wave which is transmitted through joints based on superposition of transmitted and reflected waves. These were found to perform well against numerical results. Therefore, while the values of ξ given in the previous studies are too low to be superposition effects based on Eq. (12), it is considered that the mechanism proposed previously is still correct for first arrivals.

Despite this, it is curious that this study found that values of ξ smaller than 0.5 tend to be associated with spring resonance as opposed to superposition resonance. The reason behind this is likely due to the way in which this study and previous studies approach the calculation of the transmission coefficient. Previous studies (Cai and Zhao, 2000; Zhao et al., 2006b) have taken the amplitude of the first arrival after the joint and divide this by the amplitude of the wave before the joint, with the rest of the

Table 3
Test cases and their properties. Multiple values indicate different properties for subsequent joints.

Case	ρ (kg/m^3)	C_p (m/s)	C_s (m/s)	J_n	s (m)	k_n (GPa/m)
1	2600	3328	1922	3	4, 2	3
2	2600	3328	1922	2	2	0.5, 1
3	2600	2364	1286	2	4	0.8, 0.4

Table 4
Results of validation runs in UDEC and WAVE2D for analytical models. U: UDEC, W: WAVE2D, A: Analytical.

Case	Spring resonance						Superposition resonance					
	Peak 1			Peak 2			Peak J_n			Peak $J_n + 1$		
	U	W	A	U	W	A	U	W	A	U	W	A
1	77	86	91	156	174	175	442	448	416	840	845	832
2	75	83	84	n/a	n/a	n/a	839	840	832	1663	–	1664
3	45	50	52	n/a	n/a	n/a	303	305	296	595	595	591

Note: n/a denotes a resonance that does not exist, and '-' denotes that a resonance which is not visible in the data.

Table 5
Final spring and first superposition resonant frequencies from rock masses with different numbers of joints. All rock masses have the same properties (s = 1 m, k_n = 10 GPa/m, C_p = 5830 m/s, C_s = 3840 m/s, ρ = 2650 kg/m^3).

J_n	Final spring resonance (peak $J_n - 1$) (Hz)	First superposition resonance (peak J_n) (Hz)
2	376	2915
4	492	2915
8	522	2915
11	528	2915
101	532	2915
1001	533	2915
10001	533	2915

transmitted waveform ignored. However, this study takes the full waveform before and after the joint and calculates a transfer function from these, as described in Section 2.3, by decomposing this into its harmonic components. This represents two methods of characterising the transmission of stress waves through joints, being a first arrival method, as used in previous studies, and a full waveform method, as used in this study. While it can be considered that for a first arrival, the superposition mechanism of Zhao et al. (2006b) is correct, any receptor will experience the full waveform. Therefore, for practical applications, the analytical models given in the current study are of value.

In order to test that the models considered in the current study are modelling the same problem as Zhao et al. (2006b), a set of their results has been replicated in Fig. 12. The results of Cai and Zhao (2000) and Zhao et al. (2006b) are normalised for joint stiffness, and thus cannot be directly compared to the results in this study. Therefore, a bespoke analysis was undertaken to replicate their results. Fig. 12 shows the results from Zhao et al. (2006b) for a model with two joints with a normalised joint stiffness ($k_n/(z\omega)$) of 0.494. A new model was generated to match this normalised joint stiffness and two sets of modelling results were collected. The first set modelled a single period of a 40 Hz sine wave, with the amplitude of the first arrival recorded. The second set modelled a 500 Hz Gaussian wave, with a transfer function generated based on the full waveform and the response at 40 Hz recorded. The first arrival of data is synonymous with the approach of Zhao et al. (2006b) and the full waveform synonymous with the transfer function method in this study.

The first arrival data in Fig. 12 show that the model used in this study agrees with the results from Zhao et al. (2006b). However, when the full waveform is analysed to generate a transfer function and the response at 40 Hz is taken from this, shown by the Full Waveform data, it is clear that the results of this study reveal something different to the Zhao et al. (2006b) study. The peak of the full waveform is at a different ξ and with a greater transmission coefficient than the peak of the first arrivals data. There is a low transmission portion of the full waveform data series approaching a ξ of 0.4; however, it is at a lower transmission than the first arrival data.

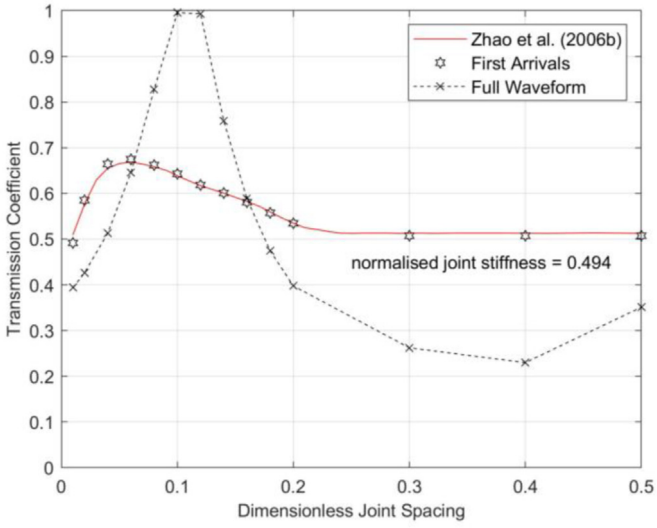

Fig. 12. Transmission coefficients for jointed rocks with J_n of 2, plotted against dimensionless joint spacing (ξ) with results from Zhao et al. (2006b) and from the current study generated using the first arrival and the full waveform.

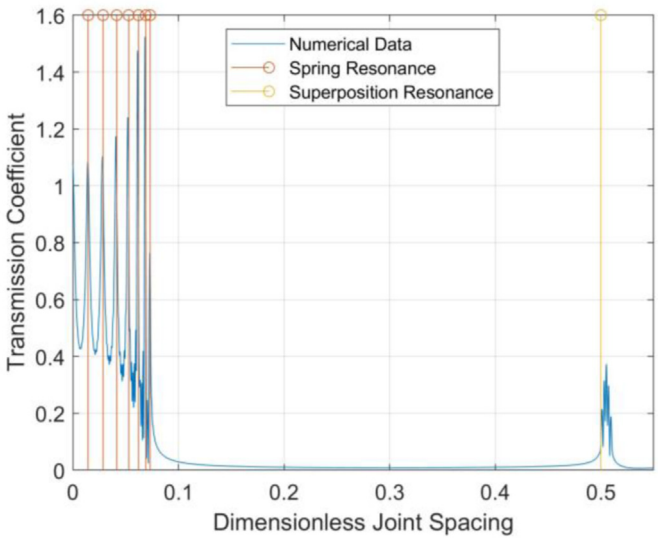

Fig. 13. Jointed rock resonance shown by a model with 8 joints (7 blocks) along with the analytical spring and superposition resonances, plotted against dimensionless joint spacing (ξ). C_p = 3328 m/s, C_s = 1922 m/s, ρ = 2600 kg/m^3, k_n = 1 GPa/m, s = 2 m, J_n = 8.

The differences exhibited highlights that different mechanisms are occurring in the rock mass when a first arrival is considered in isolation and the full transmitted waveform is analysed. In the full waveform, it is not just superposition which is occurring, and such superposition only occurs at much higher frequencies. This implies that the spring resonance mechanism is not contained within the first arrival. The spring resonance requires the blocks to oscillate, with a period given by $1/f(n)$ from Eq. (9), thus it is unlikely that these resonance mechanisms will be realised in a first arrival.

Fig. 12 shows that the results of Zhao et al. (2006b) appear to be appropriate for first arrivals; although, as highlighted by the newly identified jointed rock mass excitation mechanism of spring resonance identified in this study, only studying first arrivals will miss the nuances of transmission of the full waveform. This could possibly lead to a miss-identification of the frequencies of a wave that are preferentially transmitted through the rock mass.

It is clear from Fig. 12 that any resonance effects in the full waveform method are not clear. This is brought about by the use of the normalised joint stiffness. Instead of considering a range of frequencies from a single model with a constant joint spacing, each data point represents a new model with the same wave frequency and a different joint spacing. As a consequence, the clear resonant peaks identified in this study are not apparent. This is not to say that resonance cannot be shown in dimensionless terms. For instance, Fig. 13 shows the resonance of a numerical model with eight joints modelled in UDEC, along with the analytical resonances. This model does not have a constant normalised joint stiffness, but represents a transfer function for a range of frequencies for the same rock mass.

Much of this discussion has been conducted in dimensionless terms in order for an easy comparison to previous research (Cai and Zhao, 2000; Zhao et al., 2006b). However, the cases in Table 3 raise an important question regarding the use of ξ for calculating the response of a rock mass. In Case 1, there are two different joint spacings of 2 m and 4 m. A single value of s is required to calculate the resonance in dimensionless terms, as shown by Eq. (10). Dimensionless terms only work in very simple rock masses with a single joint spacing, which is unlikely in reality. Therefore, for application to more realistic rock masses, it is considered that

dimensional terms are most useful, giving resonance in terms of frequency.

For superposition resonance, a joint spacing is required for the calculation of the resonant frequency in Eq. (11), which is not required for the dimensionless version in Eq. (12). With multiple joint spacings, such as in Case 1, there could be multiple superposition resonances at the same ξ, although they will occur at different frequencies. Care must be taken with superposition resonance to calculate the resonances for each joint spacing within the rock mass.

The apparent agreement of the models of Zhao et al. (2006b) and this study implies that if the full waveform was analysed, then the resonance effects found here would have been identified in the previous study as well. Zhao et al. (2006b) do not give clear time series for the full waveform; however, these are given by Cai and Zhao (2000) and are reproduced here in Fig. 14, as well as by Li et al. (2012), Fan et al. (2022) and Xu et al. (2022). Cai and Zhao (2000) give these in dimensionless terms for time, joint spacing and joint stiffness, thus it is not possible to directly calculate the resonances from the full waveform. Despite this, there are clear oscillations occurring in the transmitted wave in the plots given.

Fig. 14 shows the initial wave in each of the plots followed by oscillations. These are most clearly shown in Fig. 14b and c, although they are evident in all of the plots. The dimensionless period of the oscillations seems to reduce as the relative joint spacing reduces, with the largest relative joint spacing in Fig. 14a, and the smallest in Fig. 14d. As the joint spacing reduces, assuming all other properties of the model are the same, resonance of the models will occur at a higher frequency. With two joints, there will be a single spring resonance, although there will also be additional superposition resonant frequencies. The superposition resonance would be at a very high frequency when the joint spacing is small, but this will reduce as the joint spacing increases. This will lead to the spring and superposition resonances overprinting on each other in the transmitted waveform, which could be evident in the complex time series given in Fig. 14a for the largest joint spacing.

The two resonance mechanisms, of spring and superposition resonances, have been identified and discussed in this study. Both mechanisms have been shown to operate in two different numerical modelling software with different input waves, treatment of joints and model dimensions. The analytical equations derived have been shown to accurately predict the resonant frequencies of these models and are adaptable enough to handle complex rock masses with a range of joint spacings and joint stiffnesses. The superposition resonance mechanism is a reasonably well recognised effect, being found by Nakagawa (1998), and having national standard written for their identification (BS EN 14146:2004, 2004). Anecdotal evidence of the spring resonance mechanism being observed in previous studies (Cai and Zhao, 2000) is identified in Fig. 14. Despite this, no physical experiments have been found which show the spring resonance mechanism. This is a clear omission in the research presented here, although undoubtedly the spring resonance effect occurs in numerical modelling, as shown in Fig. 11. If this is a yet unknown numerical modelling artefact, its presence should be taken into account in modelling associated with vibrations. However, it does show the need for physical experiments to verify the physical reality of the spring resonance mechanism.

6. Conclusions

This study has modelled multiple jointed rock masses in the combined discrete element-finite difference method and the finite difference method, using the codes UDEC and WAVE2D, respectively. The numerical models have been verified by replicating previous studies using the magnitude of first arrivals. Rock masses have been excited by a plane wave and transfer functions have been derived for waves that propagate through the joints using the full waveform. Analysing the full waveform, which is an approach which has not been used by previous studies, shows the presence of resonance. Superposition resonance, which has previously been found, has been shown to occur, and for the first time, a spring

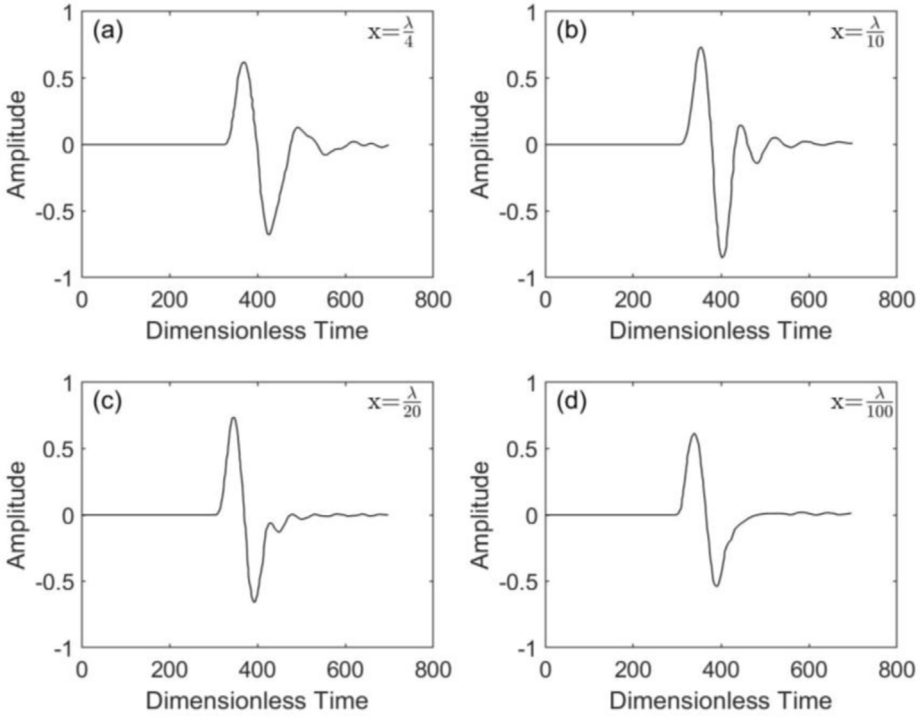

Fig. 14. Transmitted waveforms from numerical model with two joints from Cai and Zhao (2000). *X* represents the joint spacing relative to wavelength (λ) of incident sine wave.

resonance mechanism has been isolated. Analytical equations were developed for these resonance mechanisms based on classical mechanics. The mechanisms were verified using a second numerical experiment by modelling a frequency sweep in order to show that the response of the model changes when an excitation at a resonant frequency is applied.

Two distinct mechanisms have been identified, one operating at lower frequencies and another operating at relatively high frequencies. Resonance at low frequencies, referred to in this study as spring resonance, is found to operate as masses between springs and resonance at relatively high frequencies, referred to in this study as superposition resonance, is created by the superposition of multiple reflected waves within blocks. The analytical functions are closed-form, exact and able to predict the resonant frequencies for jointed materials with any properties and joint spacings, providing an efficient method for the calculation of resonant frequencies of any arbitrary jointed materials. The outcomes of this study have consequences for future analysis of the transmission of stress waves through jointed materials as neglecting the full waveform will miss the frequencies that are preferentially transmitted through multiple joints. Further validation of the effects is highlighted, with the need for a physical experiment to verify the spring resonance mechanism.

Declaration of competing interest

The authors declare that they have no known competing financial interests or personal relationships that could have appeared to influence the work reported in this paper.

Acknowledgments

This work was supported by the Engineering and Physical Sciences Research Council (EPSRC) (EP/R513258/1).

Appendix A. Supplementary data

Supplementary data to this article can be found online at https://doi.org/10.1016/j.jrmge.2022.09.001.

References

Ariga, T., Kanno, Y., Takewaki, I., 2006. Resonant behaviour of base-isolated high-rise buildings under long-period ground motions. Struct. Des. Tall Special Build. 15 (3), 325–338.
BS EN 14146:2004, 2004. Natural Stone Test Methods - Determination of the Dynamic Modulus of Elasticity (By Measuring the Fundamental Resonance Frequency). British Standards Institution, London, UK.
Barbosa, N.D., Caspari, E., Rubino, J.G., Greenwood, A., Baron, L., Holliger, K., 2019. Estimation of fracture compliance from attenuation and velocity analysis of full-waveform sonic log data. J. Geophys. Res. Solid Earth 124 (3), 2738–2761.
Cai, J.G., Zhao, J., 2000. Effects of multiple parallel fractures on apparent attenuation of stress waves in rock masses. Int. J. Rock Mech. Min. Sci. 37 (4), 661–682.
Connolly, D.P., Marecki, G.P., Kouroussis, G., Thalassinakis, I., Woodward, P.K., 2016. The growth of railway ground vibration problems - a review. Sci. Total Environ. 568, 1276–1282.
Deng, X.F., Zhu, J.B., Chen, S.G., Zhao, J., 2012. Some fundamental issues and verification of 3DEC in modeling wave propagation in jointed rock masses. Rock Mech. Rock Eng. 45 (5), 943–951.
Eitzenberger, A., 2012. Wave Propagation in Rock and the Influence of Discontinuities. PhD Thesis. Luleå Tekniska Universitet, Luleå, Sweden.
Fan, Z., Zhang, J., Xu, H., Wang, X., 2022. Transmission and application of a P-wave across joints based on a modified g-λ model. Int. J. Rock Mech. Min. Sci. 150, 104991.
Flores, J., Novaro, O., Seligman, T.H., 1987. Possible resonance effect in the distribution of earthquake damage in Mexico City. Nature 326 (6115), 783–785.
Hanson, C., Towers, D., Meister, L., 2012. High-speed Ground Transportation Noise and Vibration Impact Assessment. HMMH Report 293630-4. Office of Railroad Development, Federal Railroad Administration, U.S. Department of Transportation, Washington, D.C., USA.
Hildyard, M.W., 2007. Manuel Rocha Medal Recipient Wave interaction with underground openings in fractured rock. Rock Mech. Rock Eng. 40 (6), 531–561.
Hildyard, M.W., Daehnke, A., Cundall, P.A., 1995. WAVE: a computer program for investigating elastodynamic issues in mining. In: Proceedings of the 35th US Symposium on Rock Mechanics (USRMS). Reno, Navada, USA.
Itasca, 2014. UDEC - Universal Distinct Element Code Version 6.0. Itasca Consulting Group Inc., Minneapolis, USA.
Li, J.C., Li, H.B., Ma, G.W., Zhao, J., 2012. A time-domain recursive method to analyse transient wave propagation across rock joints. Geophys. J. Int. 188 (2), 631–644.
Li, S., Tian, S., Li, W., Yan, T., Bi, F., 2019. Research on the resonance characteristics of rock under harmonic excitation. Shock Vib. 2019, 6326510.
Ma, G.W., Fan, L.F., Li, J.C., 2013. Evaluation of equivalent medium methods for stress wave propagation in jointed rock mass. Int. J. Numer. Anal. Methods GeoMech. 37 (7), 701–715.
Mucciarelli, M., Masi, A., Gallipoli, M.R., et al., 2004. Analysis of RC building dynamic response and soil-building resonance based on data recorded during a damaging earthquake (Molise, Italy, 2002). Bull. Seismol. Soc. Am. 94 (5), 1943–1953.
Nakagawa, S., 1998. Acoustic Resonance Characteristics of Rock and Concrete Containing Fractures. PhD Thesis. University of California, Berkeley, CA, USA.
Parastatidis, E., Hildyard, M.W., Stuart, G.W., 2017. Modelling P-wave propagation in a medium with multiple parallel fractures and direct comparison with experimental recordings. In: Proceeding of the 51st US Rock Mechanics/Geomechanics Symposium. San Francisco, California, USA.
Pyrak-Nolte, L.J., Myer, L.R., Cook, N.G.W., 1990a. Anisotropy in seismic velocities and amplitudes from multiple parallel fractures. J. Geophys. Res. Solid Earth 95 (B7), 11345–11358.
Pyrak-Nolte, L.J., Myer, L.R., Cook, N.G.W., 1990b. Transmission of seismic waves across single natural fractures. J. Geophys. Res. Solid Earth 95 (B6), 8617–8638.
Schoenberg, M., 1980. Elastic wave behavior across linear slip interfaces. J. Acoust. Soc. Am. 68 (5), 1516–1521.
Wang, L., Wu, C., Fan, L., Wang, M., 2022. Effective velocity of reflected wave in rock mass with different wave impedances of normal incidence of stress wave. Int. J. Numer. Anal. Methods GeoMech. 46 (9), 1607–1619.
Xu, C., Liu, Q., Wu, J., Deng, P., Liu, P., Zhang, H., 2022. Numerical study on P-wave propagation across the jointed rock masses by the combined finite-discrete element method. Comput. Geotech. 142, 104554.
Yau, J.D., 2001. Resonance of continuous bridges due to high speed trains. J. Mar. Sci. Technol. 9 (1). https://doi.org/10.51400/2709-6998.2430.
Zhang, P., Nordlund, E., Swan, G., Yi, C., 2019. Velocity amplification of seismic waves through parallel fractures near a free surface in fractured rock: a theoretical study. Rock Mech. Rock Eng. 52 (1), 199–213.
Zhao, J., Cai, J.G., Zhao, X.B., Li, H.B., 2006a. Experimental study of ultrasonic wave attenuation across parallel fractures. Geomech Geoengin. 1 (2), 87–103.
Zhao, J., Zhao, X.B., Cai, J.G., 2006b. A further study of P-wave attenuation across parallel fractures with linear deformational behaviour. Int. J. Rock Mech. Min. Sci. 43 (5), 776–788.
Zhao, X., Zhao, J., Cai, J., Hefny, A.M., 2008. UDEC modelling on wave propagation across fractured rock masses. Comput. Geotech. 35 (1), 97–104.
Zheng, Y., Chen, C., Liu, T., Zhang, W., 2020. Numerical study of P-waves propagating across deep rock masses based on the Hoek-Brown model. Int. J. GeoMech. 20 (2), 4019152.
Zhu, J.B., Zhao, X., Li, J.C., Zhao, G., Zhao, J., 2011. Normally incident wave propagation across a joint set with the virtual wave source method. J. Appl. Geophys. 73 (3), 283–288.

Harry Holmes obtained his BSc degree in Geology and Physical Geography from the University of Edinburgh and MSc degree in Engineering Geology from the University of Leeds, in 2014 and 2016, respectively. He is currently a PhD candidate in Rock Mechanics at the University of Leeds. He previously worked as an Engineering Geologist with AECOM. His research interests include (1) numerical modelling of rock engineering problems focussing on tunnel excavation and rock dynamic; and (2) analysis of big data.